Blue-Fluorescent Antibodies

Anton Simeonov,[1] Masayuki Matsushita,[1] Eric A. Juban,[2] Elizabeth H. Z. Thompson,[3] Timothy Z. Hoffman,[1] Albert E. Beuscher IV,[1,2] Matthew J. Taylor,[1] Peter Wirsching,[1] Wolfgang Rettig,[4] James K. McCusker,[2] Raymond C. Stevens,[3] David P. Millar,[3] Peter G. Schultz,[1] Richard A. Lerner,[1] Kim D. Janda[1]

The forte of catalytic antibodies has resided in the control of the ground-state reaction coordinate. A principle and method are now described in which antibodies can direct the outcome of photophysical and photochemical events that take place on excited-state potential energy surfaces. The key component is a chemically reactive optical sensor that provides a direct report of the dynamic interplay between protein and ligand at the active site. To illustrate the concept, we used a *trans*-stilbene hapten to elicit a panel of monoclonal antibodies that displayed a range of fluorescent spectral behavior when bound to a *trans*-stilbene substrate. Several antibodies yielded a blue fluorescence indicative of an excited-state complex or "exciplex" between *trans*-stilbene and the antibody. The antibodies controlled the isomerization coordinate of *trans*-stilbene and dynamically coupled this manifold with an active-site residue. A step was taken toward the use of antibody-based photochemical sensors for diagnostic and clinical applications.

Although most biological processes occur on the thermally controlled ground-state surface, photochemical reactions involving molecular excited states are fundamental in nature, as in photosynthesis. Similarly, the physics and chemistry of vision are mediated by the light-induced double-bond isomerization of 11-*cis*-retinal bound to the protein rhodopsin (*1*). Recently, theoretical and experimental advances have made it possible to visualize how vibronic modes between proteins and ligands are coupled during movement across a potential energy surface (*2*–*4*). The application of modern spectroscopic techniques to photon-driven reactions, as well as other nonphotochemical systems, has allowed the observation of ultrafast and efficient mechanisms and shed light on a crucial paradigm for catalysis. Namely, protein-ligand interactions are dynamic and intimately dependent on the transfer of vibrational energy.

We were interested in applying catalytic antibody technology (*5*, *6*) to explore how excited states might be influenced by protein-ligand interactions. We hypothesized that because antibodies can translate binding energy along the thermal ground-state surface to lower activation barriers, similar control might also direct the pathways of molecules in electronically excited states. We used a ligand that had photochemical reactivity as an optical sensor to directly report on the interplay between the properties of a protein active site and a chemical event. We prepared a series of monoclonal antibodies (mAbs) against *trans*-stilbene **1** (Fig. 1), a molecule whose excited-state behavior is well understood (*7*–*9*). Remarkably, even though the mAbs were made to *trans*-stilbene in its ground-state structure, they could still respond dynamically to increases in molecular energy and influence the course of excited-state reactions.

Principle and design. Two decay processes, fluorescence and isomerization to *cis*-stilbene **5**, account for the excited-state behavior of **1** in solution (Figs. 1 and 2). The isomerization pathway is the predominant funnel for quenching of fluorescence at room temperature. The singlet mechanism for the trans → cis photoisomerization was proposed by Saltiel (*10*) and was validated through comprehensive singlet and triplet quenching studies (*9*). The fundamental model suggests that after excitation of the trans form to the excited trans-singlet state ($^1t^*$), twisting about the carbon-carbon double bond converts the molecule into the excited perpendicular singlet state ($^1p^*$). Subsequently, internal conversion to the perpendicular ground state (^1p) followed by rotational relaxation to the cis and trans ground states completes the process. The trans → cis photoisomerization occurs from an angle of twist of 0° to 90° by rotating in S_1 and from 90° to 180° in the S_0 state. The reverse occurs for the cis → trans reaction (Fig. 2).

Although it should be possible to elicit mAbs highly specific for the parent *trans*-stilbene **1**, we desired a derivative more suitable for experiments in aqueous media. Hence, the design required a functional group on **1** that would (i) afford coupling to a carrier protein, (ii) enhance water solubility, (iii) be stable during routine irradiation, and (iv) introduce minimal alteration of the electronic nature of **1**. The last requirement would allow us to apply the vast body of information available for *trans*-stilbene to a substituted analog. A glutaric amide was considered an ideal candidate and resulted in the preparation of hapten **2** (Fig. 1) (*11*). The Hammett σ value provides a measure of the degree to which substituents perturb the electronic nature of an aromatic ring (*12*). For the related acetamido group, $\sigma_p = -0.01$, close to the zero value assigned to hydrogen, which suggests that **2** is electronically comparable to **1**. Immunization with a keyhole limpet hemocyanin (KLH) conjugate of **2** resulted in a panel of 15 mAbs for analysis (*11*, *13*).

The fluorescence quantum yield (ϕ_f) of flexible molecules that can undergo facile torsional displacements in the excited-singlet state increases greatly in high-viscosity or low-temperature, rigid media. Hence, for **1**, there is an increase in fluorescence efficiency with a concurrent decrease in the efficiency of trans → cis photoisomerization (*14*, *15*). Similarly, when substitutions are made that constrain or "stiffen" the structure of **1** from twisting as in **10**, the isomerization yield is zero and the ϕ_f approaches unity (*16*, *17*). If the confines of a specific antibody binding site imparted "stiffness" to **2**, then we would expect a reduction in isomerization and an enhanced ϕ_f. However, the outcome could not be predicted and was quite unexpected.

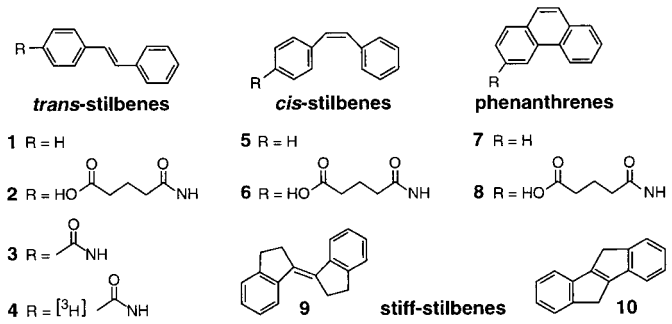

Fig. 1. Structures of compounds under discussion.

[1]Department of Chemistry, The Scripps Research Institute and the Skaggs Institute for Chemical Biology, 10550 North Torrey Pines Road, La Jolla, CA 92037, USA. [2]Department of Chemistry, University of California Berkeley, Berkeley, CA 94720–1460, USA. [3]Department of Molecular Biology, The Scripps Research Institute, 10555 North Torrey Pines Road, La Jolla, CA 92037, USA. [4]Institute of Physical and Theoretical Chemistry, Humboldt-University Berlin, Bunsenstrasse 1 D-10117 Berlin, Germany.

Initial observations. When the mAbs were each mixed with **2** in stoichiometric amounts and irradiated with ultraviolet (UV) light, a surprising phenomenon was observed. Several mAbs, 19G2, 20F2, 21C6, and 22B9, complexed with **2** immediately produced an intense, powder-blue–colored fluorescence (Fig. 3). Moreover, the panel of mAb complexes revealed a range of visually discernible colors and/or intensities over the purple (violet) to blue region of the spectrum. Similar results were found with **1** but were less marked because the concentrations were lower. By itself, **2** showed only very faint purple fluorescence typical of that for *trans*-stilbene in solution at room temperature. Because the mAbs themselves afforded no observable fluorescence, we concluded that mAb-**2** complexes were the source of the emitted light.

The distinct fluorescence of a blue-emitting complex such as 19G2-**2** was extremely robust in that there was no visible effect upon saturation with oxygen, variation of the pH from 4 to 11, a change in temperature from −5° to 50°C, or prolonged irradiation. Complete photobleaching to a colorless and turbid solution occurred only after 60 min of continuous UV exposure under the conditions described (Fig. 3). Yet, remarkably, freezing a solution of a blue-antibody complex in either a dry ice–isopropanol bath (sample temperature −60°C, 213 K) or liquid nitrogen bath (sample temperature −179°C, 94 K) followed by UV irradiation resulted in the complete absence of the blue fluorescence that reappeared only upon thawing. In the frozen state in buffer solution, the 19G2-**2** complex was a semitranslucent frozen solution in which the faint emission appeared as a purple color. This emission was similar to that of a frozen sample of the stilbene **2** alone or a room temperature or frozen sample of a typical purple-emitting complex such as 16H10-**2**. The loss of the intense blue color was counterintuitive, given the normal enhancement of fluorescence at low temperatures.

A number of hypotheses for the origin of the unusual blue fluorescence were considered (*18*). At this stage, not yet having obtained structural data for an antibody-hapten complex, we conjectured that exciplex-like interactions of **2** at the combining site could be responsible. An exciplex is a cooperative interaction of two molecules in the excited state. The new excited-state complex ("exciplex") can emit a photon to produce light. However, given the observed temperature-dependent phenomenon, it was apparent that simple static interactions between stilbene and antibody were not sufficient to produce the blue fluorescence. We suspected that dynamic events were operative and sought further evidence to support this view.

Steady-state analysis: Spectroscopy and energetics. Determination of dissociation constant (K_d) values for the *trans*-stilbene **2** quickly revealed no extraordinary tight binding effects in the ground state and no substantial differences between the blue-fluorescent mAbs and the majority of the other mAbs in the panel (Table 1). In fact, although some purple mAbs were among those with the worst affinities, the most weakly purple-fluorescent complexes of mAbs 16H10 and 9E11 had K_d values comparable to the blue-emitting complexes. However, a striking contrast was observed in the ϕ_f values as well as differences in the absorption, excitation, and emission spectra of the blue-fluorescent mAb complexes (Table 2).

The room-temperature absorption spectrum of the 19G2-**2** complex was slightly redshifted compared with free **2** and showed a vibronic progression of 0-0 and 0-1 subbands and a 0-2 subband as an inflection (Fig. 4A). The spectrum differed from that of **2**, which showed very small inflections, that of 25E5-**2**, which lacked the 0-2 subband, and that of 16H10-**2**, which was featureless. The identification of vibronic bands was somewhat similar to, but much less defined, than those of **1** in viscous or low-temperature glassy media and stiff stilbenes **9** and **10** at room temperature (*14*, *19*). The data suggested that **2** bound to 19G2 had a distinctive interaction with the antibody in the ground state and was more planar and had less phenyl torsion in the ground and/or Franck-Condon excited states than free **2** or the blue-purple or purple complexes. The excitation spectrum of the 19G2-**2** complex showed structure analogous to the absorption spectrum (Fig. 4B). Emission of blue-fluorescent mAbs was broad and featureless, similar to the band shape of **2** and other EP2 complexes, but with a redshifted maximum at 410 nm that gave rise to the color that characterized

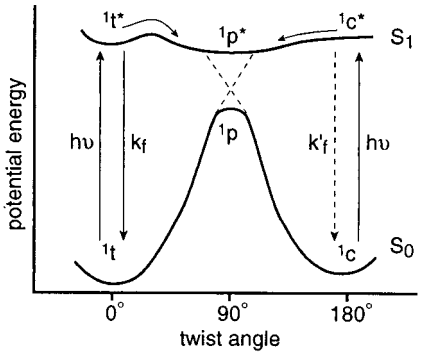

Fig. 2. Illustration of the ground- and excited-state potential energy surfaces (S_0 and S_1) for stilbene photochemistry and photophysics. The diagram is the simplest representation of the energy changes for the principal pathways of isomerization and fluorescence in the singlet excited state (t, *trans* isomer; c, *cis* isomer; p, 90° twisted state; k_f, fluorescence rate constant). Emission from *cis*-stilbene in fluid solution can only be detected and measured under special conditions but suggests that the trans and twisted minima are nearly isoenergetic (*38*, *39*).

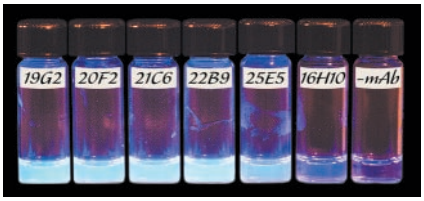

Fig. 3. Representative EP2 mAbs complexed with **2** and photographed during illumination with UV light (*11*). All samples contained 10 μM mAb, except for the background (labeled -mAb), and 20 μM **2** in a volume of 600 μl of phosphate-buffered saline (PBS) [10 mM sodium phosphate and 150 mM NaCl (pH 7.4)] and 5% dimethylformamide (DMF) cosolvent. Photographic parameters were adjusted to capture the blue fluorescence. However, photographs could not fully reproduce the color intensity or distinguish simultaneously across the range of blue and purple tones as perceived by the eye. Samples 19G2, 20F2, 21C6, and 22B9 were a more highly luminous powder-blue color than shown. Sample 25E5 was a pale blue with a purple hue and the 16H10 complex was a faint purple color. The image of the background sample was considerably distorted and to the eye had only a barely perceptible purple hue.

Table 1. Steady-state thermodynamic parameters for EP2 mAbs. All reactions were conducted in PBS [10 mM sodium phosphate and 150 mM NaCl (pH 7.4)] and 5% DMF cosolvent, at 21°C. IgG, immunoglobulin G.

EP2 mAb	IgG isotype	$K_{d,trans}$* (μM)	$K_{d,cis}$† (μM)	$[trans/cis]_{pss}$ (%)
19G2	$\kappa\gamma_{2b}$	0.16	1.7	97/3
20F2	$\kappa\gamma_{2b}$	0.30	3.8	97/3
21C6	$\kappa\gamma_{2b}$	0.20	1.6	95/5
22B9	$\kappa\gamma_{2a}$	0.25	1.6	93/7
25E5	$\kappa\gamma_{2a}$	0.18	1.4	96/4
16H10	$\kappa\gamma_{2a}$	0.31	2.3	69/31
9E11	$\kappa\gamma_{2a}$	0.20	0.10	80/20

*$K_{d,trans}$ was determined directly for **4** by equilibrium dialysis (*11*). The K_d values for **2** were about the same (±10%) as measured by competition equilibrium dialysis versus **4**. †$K_{d,cis}$ was determined by competition equilibrium dialysis of **6** versus **4**. All K_d values were accurate to ±10%.

these four mAbs (Fig. 4C). The strong emission and its spectral location were in stark contrast to free **2**, which in fluid solution emitted in the near UV with a ϕ_f that was 30- to 40-fold lower (Table 2). The change in overall appearance of the emission spectrum relative to the structured emission typically observed for *trans*-stilbene **1** as well as **2** in low-temperature rigid media (see below) suggested that the mAb caused a perturbation of the electronic structure of **2** and that the emission was due to a complex in the excited state. The 11 other EP2 mAbs gave rise to a smaller spectral shift (blue-purple and purple emission) and a lower ϕ_f of the overall emission. This finding further underscored the notable behavior of **2** bound to a blue-fluorescent mAb.

Somewhat unexpectedly, the panel of EP2 mAbs bound the *cis*-isomer **6** (Table 1) (*11*). In general, the affinities were reduced, with K_d values that were ~10-fold higher. One interesting exception was mAb 9E11, in which the K_d of the cis isomer was in fact slightly lower than that of the trans isomer. In retrospect, the cis-binding results were rationalized in light of the linker length of **2** used for immunoconjugate formation and immunization (*20*). On the basis of the results, the possibility for interconversion of the two isomers at the antibody combining site was investigated.

First, the ground-state thermal effect of EP2 mAbs on **2** at 45°C was examined. No evidence was found for the formation of **6** or any other new compound by either an exemplary blue-fluorescent mAb 19G2 or a purple-fluorescent mAb 16H10, which was expected in that the mAbs were elicited with a ground-state structure that contained no information about the transition state for catalysis of stilbene isomerization. Moreover, the ground-state barrier between trans and cis isomers of stilbene is rather large at ~43 kcal/mol (*21*) and precluded spontaneous isomerization of **2** at the maximum temperature (45° to 50°C) that maintained antibody binding. Although we could not rule out energy perturbations of the barrier or twist angles on the ground-state surface, such effects were likely to be small and only minor contributors to the phenomenon of blue fluorescence.

Second, the photostationary state (pss) of **2** and **6** in the absence and presence of EP2 mAbs was measured (Table 1). The photoisomerization of either the trans or cis isomer alone in buffer solution at room temperature with the UV transilluminator (Fig. 3) produced an excess of *cis*-isomer **6** similar to the behavior of **1** and **5** in most solvents for excitation wavelengths >300 nm (*9*, *22*). Yet, in all cases, and especially blue-fluorescent mAb complexes, the final pss at the antibody active site favored the *trans*-isomer **2**. Previous studies by others showed that in addition to **1** and **5** starting from either isomer, a minor photoproduct, dihydrophenanthrene, could form from the excited *cis*-stilbene through electrocyclization (*23*). Although the latter process is reversible, the dihydrophenanthrene readily oxidizes to phenanthrene **7** when oxygen is not excluded. Indeed, we detected the formation of **8** under normal conditions of sample preparation and irradiation in the presence of room air and surmised that this reaction manifold contributed to the bleaching of the blue fluorescence (see above) (*24*). The compound **8** also served as a marker that indicated small temperature-dependent effects on the pss (*25*). Hence, the pss was actually a metastable equilibrium continuously shifted by the electrocyclization and irreversible dihydrophenanthrene oxidation, as well as other photodegradative pathways (*24*).

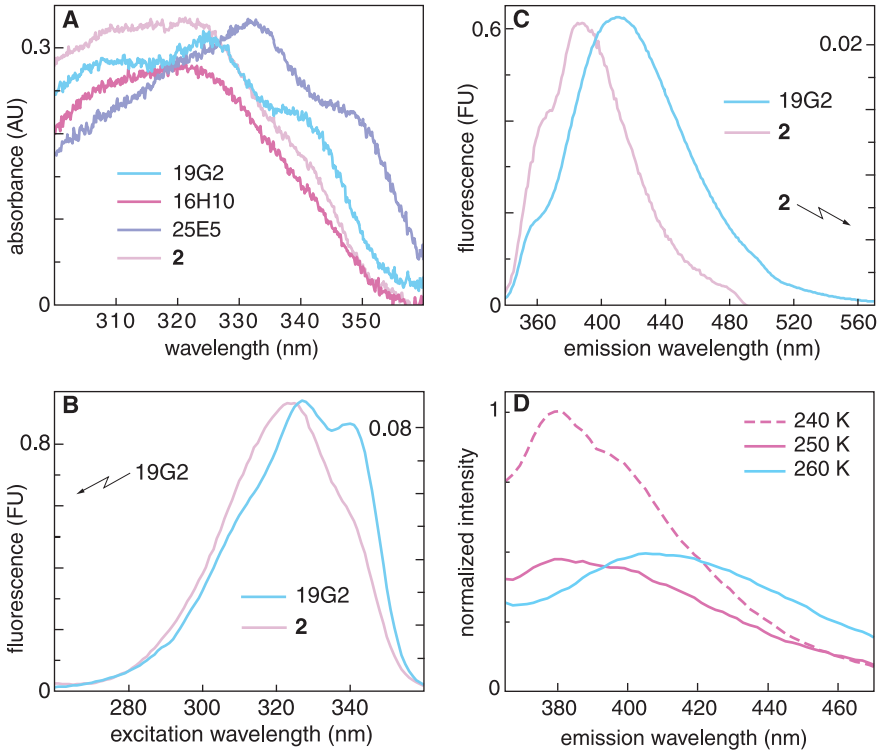

Fig. 4. Steady-state spectra. (**A**) UV absorption. (**B**) Fluorescence excitation. The 19G2-**2** complex and free **2** each required a separate *y* axis scale for side-by-side comparison of peak shapes. (**C**) Fluorescence emission. Separate *y* axes were required, as in (B). In all cases, see Table 2 for experimental conditions. Steady-state excitation and emission spectra were recorded with an SLM 8100 spectrofluorimeter (Spectronics Instruments) with a band pass of 4 nm for excitation and emission. (**D**) Low-temperature transition in blue-fluorescent antibodies. Measurements were made with either 19G2-**2** or 20F2-**2** complexes with similar results (*11*).

Table 2. Steady-state spectral data for mAb complexes and stilbenes. Unless otherwise noted, all measurements were made in PBS [10 mM sodium phosphate and 150 mM NaCl (pH 7.4)] and 5% DMF cosolvent, at 20°C (*11*). Antibody complexes were made with 20 μM mAb and 10 μM **2**. Quinine bisulfate in 0.5 M H_2SO_4 was used as a quantum yield reference with $\phi_f = 0.546$ (*43*). Fluorescence emission spectra were collected for all complexes, free stilbenes, and quinine sulfate from at least two different excitation wavelengths (313 nm and 327 nm). The quantum yields were accurate to ±10%.

EP2 mAb	λ_{em} (nm)	λ_{ex} (nm)	UV absorption bands (nm)*	$\varepsilon_{max} \times 10^{-4}$ (M^{-1} cm^{-1})	ϕ_f
19G2	410	327, 340	(310), 325, (340)	3.15	0.78
20F2	410	327, 340	(310), 325, (340)	3.15	0.80
22B9	410	327, 340	(310), 325, (340)	3.00	0.69
21C6	410	327, 340	(310), 325, (340)	3.18	0.64
25E5	387	334, 347	332, (349)	3.32	0.63
16H10	380	327	320	2.82	0.28
2	388	325	320	3.32	0.02
9	442	336, 353	340, (361)	3.00	nd†
10	362‡	317, 330	(310), 323, (344)	2.22	nd†

*The values in parentheses were observed as shoulders or inflections. †nd, not determined. ‡A second band was observed at 381 nm. In 2-methylcyclohexane, two bands were observed (356 nm and 376 nm).

Both geometric restrictions and the effective polarity of a binding site can influence the relaxation pathways of a molecule in an excited state and alter the outcome of a reaction. Inclusion of *trans*-stilbene in β-cyclodextrin was previously examined by steady-state methods and found to favor a trans pss yet showed no enhancement of fluorescence (*26*). However, an antibody binding site programmed by hapten design should be much more specific, dynamic, and chemically complex than a cyclodextrin cavity. Although a "lock and key" paradigm that invoked "freezing out" motions of **2** at the active site could in principle explain the increased ϕ_f values relative to **2** in buffer solution, the data do not support such a model. The absence of well-defined vibronic structure of absorption and emission bands was not indicative of a stilbene molecule with a rigidity able to furnish the $\phi_f \sim 0.7$ to 0.8 of blue-fluorescent complexes. In this regard, the available binding energy of ~8 to 9 kcal/mol should be sufficient to restrict the single-bond phenyl torsions ($\ll$0.1 kcal/mol), but not the isomerization motion at the high energy of the excited state.

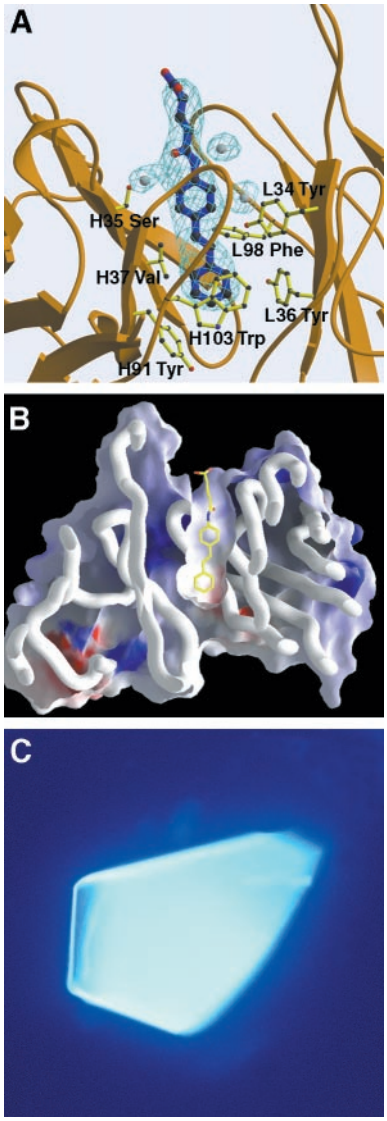

Fig. 5. (**A**) View of the stilbene hapten **2** bound to Fab 19G2. Only side chains within 5 Å of the hapten are shown. The $F_o - F_c$ electron density map was contoured at 2.0σ. Gray spheres represent water molecules (*11*). (**B**) Electrostatic surface map of Fab 19G2. The hapten **2** bound to a relatively uncharged, hydrophobic pocket. (**C**) A crystal of the 19G2-**2** complex under UV irradiation. The crystal was mounted inverted on a depression glass slide and photographed with a Zeiss Axiophot equipped with UV and fluorescence filters. Photographs were taken at ×20 magnification with exposure times ranging from 10 to 60 s on Kodak Ektakrome ASA400 film.

Moreover, the effective viscosity at the active site of the antibody certainly should be much less than that of a frozen solvent or viscous media such as glycerol. Yet, remarkably, the ϕ_f for the 19G2-**2** complex compared favorably with the value of $\phi_f = 0.75$ for **1** at 77 K in hydrophobic solvents and at 193 K in glycerol (*14*). In essence, the structural, chemical, and dynamic characteristics of the active-site matrix recapitulated a high-friction or low-temperature "glassy" environment that drastically reduces the isomerization funnel and efficiently yields fluorescence. Even blue-purple and purple complexes maintained high trans-favored pss and ϕ_f values far greater than that of stilbene in fluid solution (Tables 1 and 2). However, for neither blue, blue-purple, nor purple mAb complexes was the vibronic structure of spectra indicative of a rigid stilbene. Despite the conformational mobility in all of these mAb complexes, the emission wavelengths were distinct. Accordingly, a picture emerged of dynamically "tuned" interactions between stilbene and mAb bound together by noncovalent forces during the photoevent.

Vital support for the dynamic dependence of the blue fluorescence was obtained from low-temperature fluorescence spectroscopy that corroborated initial visual observations (see above). At 100 K, a structured emission of the 19G2-**2** complex was observed comparable to that of **2** alone and reminiscent of *trans*-stilbene in rigid media (*11*, *19*). The essential vibronic features of the emission profile remained intact through 220 K. The onset of a thermal transition began at 240 K, where the intensity of the emission and vibronic pattern began to change markedly (Fig. 4D). The spectrum broadened considerably and shifted to the red, and by 260 K the evolution was complete and matched that observed at room temperature for the emission of blue-fluorescent mAb complexes. The abruptness of the temperature transition was notable, in that the bulk medium was still frozen at 260 K. Clearly, a dynamic event occurred near 250 K that allowed the conversion to the blue-emissive species. In all likelihood, structural motion and/or vibrational states of the stilbene hapten were allowed in the region of 250 K because of a glass transition (*27*) of the antibody, or specific coupled interactions between protein and hapten were activated in this temperature regime.

X-ray crystallography. Insight into the chemical environment of the antibody active site and the position of the bound hapten was obtained from crystallographic analyses. The structure of the Fab fragment of 19G2 complexed with **2** was solved to 2.4 Å resolution at 4°C (277 K) (Fig. 5, A and B) (*11*). As for the 19G2-**2** complex in solution at this temperature, the crystals glowed blue upon UV irradiation (Fig. 5C). The hapten was readily modeled into the density in a planar, trans configuration with the long axis directed toward the center of the mAb and all of the nonhydrogen atoms accounted for in an $F_o - F_c$ difference map. Most of the side chains that packed against the stilbene moiety were nonpolar in nature. Importantly, the phenyl ring distal from the linker was positioned primarily by a parallel displaced or "face-to-face" π-stacking interaction with the indole group of the heavy-chain tryptophan 103 (Kabat numbering), a residue generally invariant in the amino acid sequence of all antibodies. Indeed, Trp^{103} was also present in the sequence of the purple mAb 16H10. The central olefinic carbons of the stilbene were enclosed by heavy-chain residues Val^{37} and Ala^{93} and light-chain residues Tyr^{36} and Phe^{98} in which the hydroxyl group of Tyr^{36} was within 3.3 Å of the distal carbon. The proximal phenyl ring was positioned between the loops of complementarity-determining regions H3 and L3 with heavy-chain Gly^{95} and light-chain Pro^{96} on either side of the ring. The protein packing in the region of the proximal ring was less intimate compared with that of the distal ring. Three water molecules were anchored by main-chain and side-chain hydrogen bonds to form part of the van der Waals surface against the proximal ring. Finally, the crystallographic structure of the 19G2-**2** complex at low temperature (100 K) (*28*) indicated that main-chain and side-chain atoms of the antibody active site and the relative position of the bound stilbene were similar to that of the complex at 277 K, well above the 250 K transition temperature. Although it now seemed reasonable to invoke an exciplex involving Trp^{103}, it was also evident that blue fluorescence must arise from a dynamic interplay between the stilbene hapten and antibody in the excited state.

Dynamic spectroscopy. Picosecond time-resolved emission spectroscopy was used to further probe the dynamics of blue-fluorescent mAb complexes. Time-resolved emission decay profiles of free **2** and bound to EP2 mAbs were measured at room tempera-

ture by time-correlated single-photon counting (Table 3 and Fig. 6A). The hapten **2** in aqueous buffer exhibited a rapid decay with one fluorescence lifetime of ~70 ps, in good agreement with previous data for **1** under comparable conditions (*7*–*9*), that indicated similar excited-state decay pathways for the two molecules. A marked change in the excited-state lifetime was observed for complexes of **2** with blue-fluorescent mAbs. In striking contrast to the subnanosecond lifetime of **2** in solution, the decay profile of the complex was dominated by an unusually long lifetime of 23 ns (Table 3). However, the blue-purple (e.g., 25E5) and purple (e.g., 16H10) complexes exhibited maximum fluorescence decay times that did not exceed 2.0 ns (Table 3). In all complexes, the existence of multiple decay times probably represented heterogeneity in the ground and/or excited states (*29*).

Decay-associated spectra of a blue-fluorescent complex revealed pronounced spectral differences among the four lifetime components (Fig. 6B). The spectra corresponding to the two shortest lifetimes were centered around 380 nm, coincident with the emission spectrum of free **2** or the low-temperature (240 K) emission spectrum of the complex (Fig. 4D), whereas the spectra corresponding to the two longest lifetimes were redshifted to ~420 nm. On the basis of the redshift and the long decay times, we interpreted the 420-nm emission as an exciplex of **2** with an antibody residue that was likely Trp^{103}. The 380-nm emission we assigned to stilbene **2** itself at the antibody combining site.

Exciplex emission was further supported by the calculation of radiative lifetimes (τ_r) for blue-fluorescent complexes. The τ_r for **2** in aqueous buffer was 3.6 ns (Table 3), comparable to previous determinations of the radiative lifetime of *trans*-stilbene **1** (*30*, *31*). However, the τ_r for the blue-fluorescent mAb complexes was 30 to 40 ns or one order of magnitude larger than the intrinsic value. In contrast, the τ_r values for the blue-purple and purple complexes were similar to free **2** and not that expected of an exciplex. Long radiative lifetimes (>3.6 ns) have been observed for exciplexes and excimers of **1** in solution (*18*). Importantly, the radiative lifetime of a stilbene exciplex must be longer than that of stilbene alone because of a low quantum-mechanical probability of the transition from the exciplex state to the ground state.

Finally, the kinetics of exciplex formation was directly monitored. An examination of the long- and short-wavelength extremes of the spectrum showed that the appearance of the blue exciplex emission was coupled to the initial decay of the purple stilbene emission (Fig. 6C). Hence, excitation of **2** resulted in a short-lived stilbene fluorescence followed by evolution to a blue-emitting exciplex that persisted for tens of nanoseconds and produced more than 98% of the observed emission (Table 3).

Nature of the exciplex. We suggest that the emission of blue-fluorescent mAb complexes is due to the formation of an exciplex dynamically established between the stilbene **2** and an active-site residue during the photoevent. The most likely protein partner appears to be Trp^{103} positioned in a π-stacking orientation with respect to the distal aromatic ring of **2**. In addition, the hydrogen bonding of tyrosine hydroxyls and/or water molecules to the stilbene substrate is possible both in the ground state and the more polarizable excited state. Furthermore, on the basis of solvent-effect studies (*32*), the hydrophobic environment of the antibody active site is conducive to a charge-transfer exciplex that is stable, long-lived, and affords a high quantum yield. However, as revealed by the temperature dependence and crystal structure data, the critical aspect is that a simple static interaction between stilbene and tryptophan is not sufficient to yield the blue fluorescence.

At low temperatures (<250 K), the substrate **2** bound to 19G2 was completely restricted with regard to trans → cis isomerization. The resulting emission therefore resembled that typically observed for *trans*-stilbene in a rigid matrix such as an optical glass. As the temperature was increased, a transition occurred at ~250 K that allowed formation of the exciplex and emission of blue light. From a static viewpoint, the x-ray structural data showed no change in the overall protein structure nor any substantial repositioning of Trp^{103} relative to the stilbene in the binding site

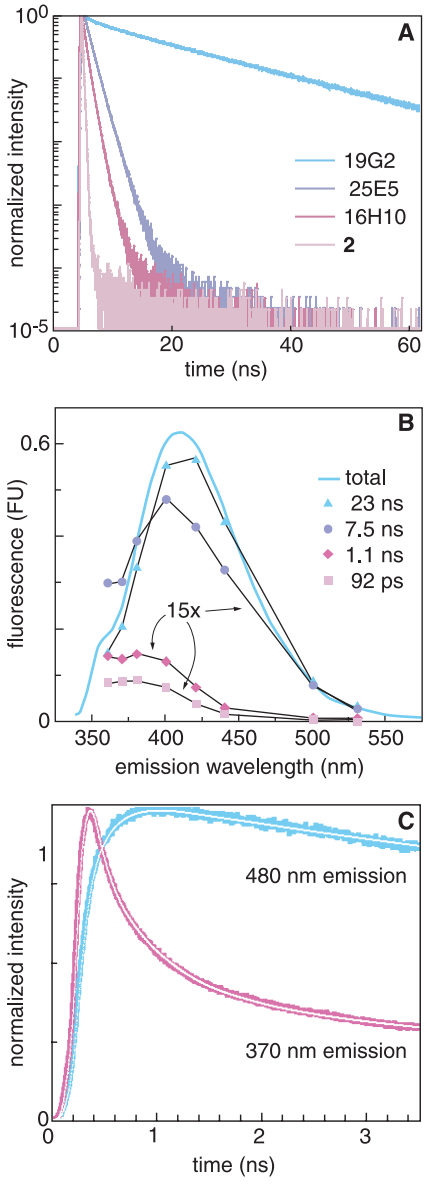

Fig. 6. Time-resolved spectroscopy. (**A**) Emission decay profiles. Measurements were obtained with picosecond excitation at 318 nm. Decays were measured at 410 nm (19G2 complex) or 380 nm (25E5 and 16H10 complexes, free **2**) by time-correlated single photon counting. Decays were recorded in 4096 channels with a time increment of 18 ps/channel and were normalized relative to the number of counts recorded in the peak channel. (**B**) Decay-associated emission spectra of blue-fluorescent mAbs. The 20F2-**2** complex was used as an example. The contribution of decay component *i* to the total emission intensity at wavelength λ, $I_i(\lambda)$, was calculated as follows: $I_i(\lambda) = [\alpha_i(\lambda)\tau_i/\Sigma_i\ \alpha_i(\lambda)\tau_i]I_{tot}(\lambda)$, where τ_i is the decay time of component *i*, $\alpha_i(\lambda)$ is the amplitude of component *i* at wavelength λ, and $I_{tot}(\lambda)$ is the total steady-state emission intensity at that wavelength. The decay parameters were obtained from multiexponential fits to the intensity decays measured at each wavelength. The spectra for the 92-ps, 1.1-ns, and 7.5-ns components were multiplied by a factor of 15 to make them visible on the same vertical axis as the 23-ns component. (**C**) Kinetic evolution of the exciplex blue emission. Normalized time-resolved emission profiles of the 20F2-**2** complex were recorded at 480 nm (blue) and 370 nm (purple). The solid lines are multiexponential fits to each decay. Emission at 480 nm showed a time-dependent increase with a rise time of 78 ± 10 ps that closely matched the initial decay time of 92 ± 10 ps observed at 370 nm. Decays were recorded in 4096 channels with a time increment of 4.9 ps/channel and were normalized relative to the number of counts recorded in the peak channel.

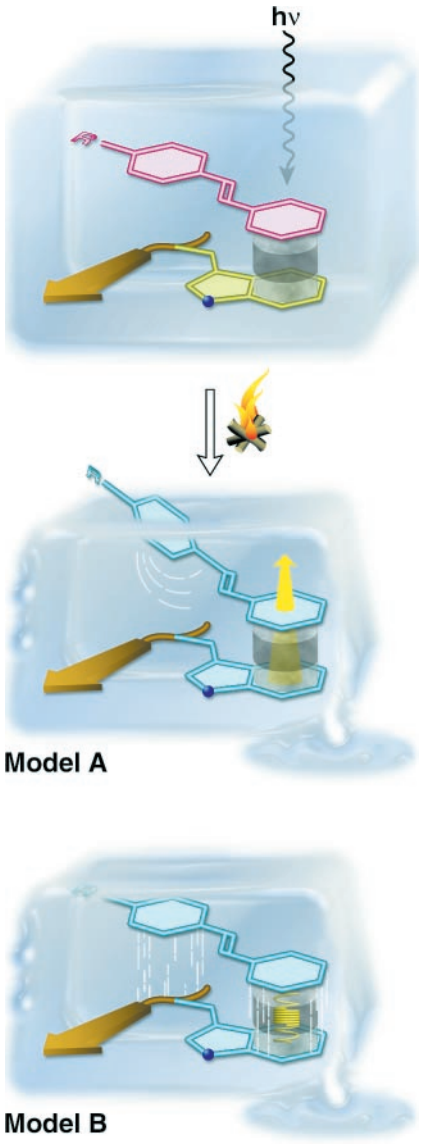

Fig. 7. Depiction of models for exciplex formation. In the frozen state (<250 K) (top), UV irradiation produces only typical stilbene fluorescence, even though there is π-electron interaction with tryptophan. Presumably, stilbene twisting is precluded and/or appropriate vibrational forces of the complex are not activated. Upon thawing (>250 K), dynamics ensue. Model A assumes that twisting is the primary factor that induces charge transfer, although other increased vibrational modes certainly occur. Model B does not require twisting but instead only invokes specific, coupled ("spring-like") vibrations between the excited-state stilbene and antibody that cause changes in the π-overlap. In both models, the electronic perturbations result in emission from the exciplex. The crystalline complex at >250 K is not representative of the frozen state (top), but rather a state having appropriate dynamic activity.

above or below the transition temperature. Therefore, stilbene and antibody must be dynamically coupled to yield the exciplex. In fact, it was possible to follow this event

Table 3. Time-resolved data for mAb complexes and stilbenes. Unless otherwise noted, all measurements were made in PBS [10 mM sodium phosphate and 150 mM NaCl (pH 7.4)] and 5% DMF cosolvent, at 20°C (*11*). Antibody complexes were made with 20 μM mAb and 10 μM **2**. The details of the time-correlated single photon counting system used to record time-resolved fluorescence decay profiles and determine decay components are described elsewhere (*11*, *44*). The radiative lifetime (τ_r) was calculated from the fluorescence lifetime (τ_f) and quantum yield (ϕ_f) (Table 2): $\tau_r = \tau_f / \phi_f$. In the case of multiexponential fluorescence decays as observed for the EP2 complexes, a good approximation for τ_r was obtained if the decay component τ_i with the largest relative weight ϕ_f (rel, *i*) was used in a slightly modified equation: $\tau_r = \tau_i/[\phi_f\, \phi_f\, (\text{rel}, i)]$. The decay component with the largest relative weight at a given wavelength was calculated with the equation $\phi_f\, (\text{rel}, i) = (\alpha_i\, \tau_i)/(\Sigma_i\, \alpha_i\, \tau_i)$ (*45*).

EP2 mAb	Fluorescence decay components, τ_f (ns)	τ_r (ns)	k_r (ns^{-1})*	k_{nr} (ns^{-1})†
19G2	22.9, 7.6, 1.1, 0.086	31	0.032	0.0091
20F2	23.3, 7.5, 1.05, 0.092	31	0.032	0.0081
22B9	22.9, 7.2, 0.97, 0.07	36	0.028	0.012
21C6	23.2, 9.1, 1.5, 0.27	39	0.026	0.014
25E5	1.66, 1.06	2.6	0.38	0.23
16H10	0.864, 0.375	4.3	0.23	0.77
2	0.071	3.6	0.28	14
10	1.71‡	3.5	0.29	0.30

*Radiative rate constant. Calculated as the inverse of τ_r. †Nonradiative rate constant. Calculated as follows: $k_{nr} = [k_r(1 - \phi_f)/\phi_f]$. ‡Measured in 2-methylcyclohexane.

in real time, which took place in ~80 ps at room temperature. Consistent with this model was the observation of slight differences (ϕ_f and τ_r) in the emission of the four blue antibodies, because these parameters might be sensitive to the relative positions and interplay of hapten and partner residue(s) that will vary somewhat amongst mAbs. In this regard, we also cannot rule out that the exciplex resulted from a higher order ensemble of stilbene and multiple aromatic residues that were evident in the crystal structure. Although ternary or higher exciplexes would be entropically disfavored in solution, the union of hapten within the ordered protein scaffold would make tenable a scenario involving a π network. Although Trp^{103} was present in all the blue mAbs, it was also present in the purple mAb 16H10. Although the x-ray data for 16H10 remain to be acquired, the position of Trp^{103} should not be grossly different based on the consistency of antibody structure. Hence, subtle structural variations and mechanistic details were perhaps most important in dictating the photophysics and photochemistry of antibody-stilbene complexes.

A physicochemical mechanism for the blue fluorescence would imply that after photoexcitation above 250 K, the bound substrate **2** undergoes partial twisting along the trans → cis isomerization coordinate and at some point interacts with the appropriately positioned tryptophan residue (Fig. 7). Below 250 K, despite no apparent static differences in the relative positions of **2** and Trp^{103}, the motion required for creation of the exciplex was hindered and so blue fluorescence was not observed. One possible reason for efficient dynamic coupling of the two aromatic moieties would entail favorable changes in electron demand, redox potential, or dipolarization that occurred as the stilbene molecule reorganized its electronic state. An alternative mechanism does not necessitate twist relaxation but relies even more on intimate displacements, oscillations, and dispersive forces (Fig. 7). In particular, specific vibrational modes of the protein might mediate coupling between the exciplex partners. Indeed, small differences in vibrational characteristics of each mAb, and hence effects on the excited state, might be due to minor sequence variations of the active-site residues.

Although no design elements were implemented to control the excited state, blue-fluorescent mAb complexes dynamically accommodated and productively funneled a large amount of energy into a long-lived fluorescent species with little thermal loss into the protein matrix. Hence, antibodies are not only able to control energetic manifolds in the ground state but also markedly influence excited-state surfaces. Molecules that are promoted to electronically excited states by the absorption of light have a number of reaction pathways that may be traversed. Binding energy, mediated by specific amino acid contacts, can serve as a linchpin between two dynamic entities, protein and ligand. Blue-fluorescent mAb complexes revealed the exquisite capacity for a finely tuned thermochemical interaction to efficiently route an excited state to generate fluorescent light. In this regard, a step was taken toward using photochemical sensors to study the ways that proteins catalyze reactions particularly in terms of the role of protein-ligand dynamics. Practical applications should also be possible and include uses in immunochemistry, in vitro and in vivo histological assays, and genomic studies.

References and Notes

1. G. G. Kochendoerfer, S. W. Lin, T. P. Sakmar, R. A. Mathies, *Trends Biochem. Sci.* **24**, 300 (1999).
2. L. Zhu, J. T. Sage, P. M. Champion, *Science* **266**, 629 (1994).
3. Q. Wang, R. W. Schoenlein, L. A. Peteanu, R. A. Mathies, C. V. Shank, *Science* **266**, 422 (1994).
4. U. Liebl *et al.*, *Nature* **401**, 181 (1999).
5. P. G. Schultz and R. A. Lerner, *Science* **269**, 1835 (1995).
6. P. Wentworth Jr. and K. D. Janda, *Curr. Opin. Chem. Biol.* **2**, 138 (1998).
7. J. Saltiel and Y.-P. Sun, in *Photochromism: Molecules and Systems*, H. Dürr and H. Bouas-Laurent, Eds. (Elsevier, New York, 1990), pp. 64–162.
8. D. H. Waldeck, *Chem. Rev.* **91**, 415 (1991).
9. H. Görner and H. J. Kuhn, *Adv. Photochem.* **19**, 1 (1995).
10. J. Saltiel, *J. Am. Chem. Soc.* **89**, 1036 (1967).
11. Details for the preparation of compounds and mAbs methods used in spectroscopic, photochemical and structural studies, and data for all 15 mAbs (Tables 1 through 3) are available as supplementary material at *Science* Online at www.sciencemag.org/feature/data/1052306.shl.
12. O. Exner, *Correlation Analysis of Chemical Data* (Plenum, New York, 1988).
13. G. Köhler and C. M. Milstein, *Nature* **256**, 495 (1975).
14. J. Saltiel and J. T. D'Agostino, *J. Am. Chem. Soc.* **94**, 6445 (1972).
15. S. Malkin and E. Fischer, *J. Phys. Chem.* **68**, 1153 (1964).
16. J. Saltiel, A. Marinari, D. W. L. Chang, J. C. Mitchener, E. D. Megarity, *J. Am. Chem. Soc.* **101**, 2982 (1979).
17. J. Saltiel, O. C. Zafiriou, E. D. Megarity, A. A. Lamola, *J. Am. Chem. Soc.* **90**, 4759 (1968).
18. Excimer fluorescence of **1** as a ternary complex with solvent in γ-cyclodextrin (*33*) and in hybrid oligonucleotides (*34*) was reported. However, in a specific binding site generated by hapten programming, complexation of multiple stilbenes **2** would be precluded. Exciplex formation between stilbenes and amines has been thoroughly investigated [see, for example, (*35*)]. The lack of participation by primary amines tended to rule out the possible involvement of a lysine residue. Furthermore, the absence of pH effects on 19G2-**2** fluorescence also argued against dependence on a particular ionic state (i.e., charged residues) of the protein. However, we could not exclude the possibility of exciplex formation with aromatic amino acids. Finally, we did not detect the existence of a **2** radical or cation-radical species using electron-spin resonance (ESR) under steady-state irradiation [for **1**, see (*36*)].
19. Ogawa *et al.* (*37*) measured the spectra for **1**, **9**, and **10** in typically used low-temperature spectroscopic solvents 2-methylpentane and 2-methyltetrahydrofuran. In these organic solvents at room temperature, **1** showed a weak progression slightly more defined than **2** in the buffer solution. The band shapes for **1** in rigid media were much sharper and more defined than the 19G2-**2** complex, but the vibronic progression was the same. The vibronic structure for **9** at room temperature was also better defined than 19G2-**2**, and with the 0-0 band intensity equal to 0-1. For **10**, there was some additional fine structure in addition to the major bands. For **10** in buffer (Table 2), the fine structure was absent, but the progression was more defined. In our low-temperature experiments (*11*), the excitation spectrum of **2** in frozen buffer at 100 K was more defined than the 19G2-**2** complex. These workers observed that a slight redshift of the absorption spectrum of **1** occurred in more polar solvents and also for **9** and **10** compared with **1** in a particular solvent. We presumed that EP2 antibody binding sites would have a bulk dielectric constant less than that of aqueous buffer. However, localized effects were considered. Consequently, either structural phenomena or polarity effects, or both, could be invoked as the cause for the redshift in blue and blue-purple mAb complexes.
20. On the basis of empirical data from our laboratory, linker lengths of 13 to 15 Å promoted complete, high-affinity recognition of a variety of haptenic structures. Here, the linker length of **2** was about 8 Å between attachment to the KLH carrier protein and the proximal point of attachment to the stilbene framework. Consequently, during the immune response, the distal aromatic ring and the connecting double bond were probably buried in the antibody binding site and served as the primary specificity determinants, with less recognition of the proximal aromatic ring. The model suggests a discrimination between the two rings in **2** or **6**, perhaps different ground-state binding modes between *cis* and *trans* isomers, and that the proximal ring was "looser" and more subject to torsional effects.
21. G. B. Kistiakowsky and W. R. Smith, *J. Am. Chem. Soc.* **56**, 638 (1934).
22. The photostationary state composition for direct excitation of a two-isomer system under a given set of conditions is a function of the product of extinction coefficients at a particular wavelength and the isomerization quantum yields: $(\text{trans/cis})_{pss} = [\varepsilon_c(\lambda)/\varepsilon_t(\lambda)](\phi_{c\rightarrow t}/\phi_{t\rightarrow c})$. UV irradiation of the *cis*-isomer **6** in the presence of EP2 mAbs afforded the same visual fluorescence as from **2**. Spectroscopic analysis of free **6** and antibody complexes indicated nothing unusual and only an initial fluorescence from a small amount of the **2** present as an impurity. Fluorescence of **5** in fluid solution was only recently detected under special conditions (*38*, *39*). No isomerization of **2** was observed in routine spectroscopic samples as measured by high-performance liquid chromatography (Table 1) (*11*).
23. W. H. Laarhoven, in *Photochromism: Molecules and Systems*, H. Dürr and H. Bouas-Laurent, Eds. (Elsevier, New York, 1990), pp. 282–300.
24. The slower rate of formation of **8** in both the background (no mAb) and EP2 mAb reactions compared with the rate of establishment of the pss allowed a "stable" pss to be attained before substantial formation of **8**. With blue-fluorescent mAbs at room temperature, 0 to <1% **8** was detected after 30 to 40 s starting with **2** and <1 to 1% at 30 s starting with **6**. The results were similar for the other mAbs that had $(\text{trans/cis})_{pss} > 90/10$. For some mAbs with higher levels of **6** in the pss, **8** was detected at 25 s and was generally 1 to 2% at 30 s starting from **2** or **6**. In background reactions, <1 to 1% **8** was observed at 50 s starting with **2** and <1 to 1% at 40 s starting with **6**. It was proposed that the initial motion of excited **5** on the S_1 surface was toward photocyclization (*40*). The compound **8** had a $K_d > 500$ μM and so did not compete with **2** or **6** at the pss concentrations (Table 1). However, it was uncertain whether oxidation of the corresponding dihydrophenanthrene occurred at the active site or in bulk solution. The formation of **8** was one possible pathway for photobleaching. Although under the conditions of the intensity of the UV illuminator, degradation of **8** was evident at 60 s and perhaps continued almost comparably to its rate of formation. At 60 s, mass balance began to deteriorate among **2**, **6**, and **8** concomitant with the loss of fluorescence. All compounds likely underwent oxidative and nonoxidative photoreactions. By chromatographic analysis, we observed no photoproduct formation, such as stilbene photodimers, but have preliminary evidence for covalent labeling of the antibody. Notably, a sample of 19G2-**2** that was subjected to freeze-thaw evacuation cycles with argon purging and sealed in an ampoule was extremely photostable and completely bleached after 7 hours of continuous UV irradiation. Only **8** remained, indicative that some oxygen had not been removed, but only at ~15% of the initial concentration of **2**.
25. Studies indicated that the isomerization of **1** had a ~3.0 kcal/mol intrinsic barrier and was strongly influenced by solvent viscosity and to a smaller extent by temperature (*7–9*, *14*). From the cis side, isomerization has been assumed to be essentially barrierless subject only to medium-imposed factors (*7–9*). We observed only small temperature effects in pss experiments over the range −5°C to 45°C for EP2 mAbs. At 45°C, the background pss showed no change from the value at 21°C, but the pss in mAb complexes shifted ~2% in favor of *cis*-isomer **6**. At −5°C, the 19G2-**2** pss was >99% *trans*-isomer **2**, and starting from **6**, the first traces of phenanthrene **8** were observed before the establishment of the pss. Hence, formation of **8** became competitive with cis isomerization and resulted in a pss of ~98% *trans*-isomer **2**.
26. The $(\text{trans/cis})_{pss}$ was ~75/25. Syamala *et al.* (*41*) proposed that interactions between **1** and the rim of the cyclodextrin occurred at the twisted $^1p^*$ state. The *cis*-isomer **5** also isomerized and was postulated to bind in a different mode.
27. D. Vitkup, D. Ringel, G. A. Petsko, M. Karplus, *Nature Struct. Biol.* **7**, 34 (2000).
28. A. Simeonov *et al.*, data not shown.
29. Duveneck *et al.* (*42*) observed two decay times for **1** complexed with β-cyclodextrin and regarded these as average fluorescence lifetimes of loosely bound and tightly bound forms that interconverted slowly on the time scale of the photoisomerization.
30. J. Saltiel, A. S. Waller, D. F. Sears Jr., C. Z. Garrett, *J. Phys. Chem.* **97**, 2516 (1993).
31. J. B. Birks and D. J. S. Birch, *Chem. Phys. Lett.* **31**, 608 (1975).
32. J. P. Palmans, M. Van der Auweraer, A. M. Swinnen, F. C. De Schryver, *J. Am. Chem. Soc.* **106**, 7721 (1984).
33. R. A. Agbaria, E. Roberts, I. M. Warner, *J. Phys. Chem.* **99**, 10056 (1995).
34. F. D. Lewis *et al.*, *J. Am. Chem. Soc.* **117**, 8785 (1995).
35. F. D. Lewis *et al.*, *J. Am. Chem. Soc.* **117**, 660 (1995).
36. J. L. Courtneidge, A. G. Davies, P. S. Gregory, *J. Chem. Soc. Perkin Trans. 2* **1987**, 1527 (1987).
37. K. Ogawa, H. Suzuki, M. Futakami, *J. Chem. Soc. Perk. Trans. II* **1988**, 39 (1988).
38. J. Saltiel, A. S. Waller, D. F. Sears Jr., *J. Am. Chem. Soc.* **115**, 2453 (1993).
39. J. Saltiel, A. Waller, Y.-P. Sun, D. F. Sears Jr., *J. Am. Chem. Soc.* **112**, 4580 (1990).
40. H. Petek *et al.*, *J. Phys. Chem.* **94**, 7539 (1990).
41. M. S. Syamala, S. Devanathan, V. Ramamurthy, *J. Photochem.* **34**, 219 (1986).
42. G. L. Duveneck, E. V. Sitzmann, K. B. Eisenthal, N. J. Turro, *J. Phys. Chem.* **93**, 7166 (1989).
43. J. N. Demas and G. A. Crosby, *J. Phys. Chem.* **75**, 991 (1971).
44. C. R. Guest, R. A. Hochstrasser, L. C. Sowers, D. P. Millar, *Biochemistry* **30**, 3271 (1991).
45. W. Rettig, W. Majenz, R. Herter, J. F. Letard, R. Lapouyade, *Pure Appl. Chem.* **65**, 1699 (1993).

46. We thank I. Niesman for fluorescence microscopy, D. B. Goodin for ESR experiments, and G. P. McElhaney, D. Kubitz, and T. M. Jones for technical assistance. We are grateful to F. D. Lewis for helpful discussions and the Tokushima-Bunri University for a sabbatical leave (M.M.). We thank the Stanford Synchrotron Radiation Laboratory (SSRL) for data collection time. Coordinates for the 19G2-**2** complex have been deposited at the Protein Data Bank with accession number 1FL3. Supported by the NIH [GM43858 (K.D.J), AI39089 (R.C.S), and P01CA27489 (Program Project Grant)], the Skaggs Institute of Chemical Biology, and the Arthur C. Cope Scholar Award (K.D.J.).

17 May 2000; accepted 24 August 2000